Polyindene/Organo-Montmorillonite Conducting Nanocomposites. I. Synthesis, Characterization, and Electrokinetic Properties

Serkan Guzel, Halil Ibrahim Unal, Ozlem Erol, Bekir Sari

Chemistry Department, Gazi University, Smart Materials Research Lab., Ankara, Turkey

Received 4 January 2011; accepted 15 May 2011
DOI 10.1002/app.34922
Published online 1 September 2011 in Wiley Online Library (wileyonlinelibrary.com).

ABSTRACT: In this study, Na-montmorillonite was organically modified with cetyltrimethylammoniumbromide (CTAB) and intercalated with *in-situ* polymerized indene. Polyindene(PIn)/Organo-MMT nanocomposites were obtained with three different compositions and coded as: K1: [PIn(94.5%)/O-MMT(5.5%)], K2: [PIn(92.8%)/O-MMT(7.2%)], and K3: [PIn(87.9%)/O-MMT(12.1%)]. These nanocomposites were subjected to full characterization with various techniques. Electrokinetic studies were conducted to reveal the zeta (ζ)-potential characteristics of the nanocomposites. ζ-potentials of the materials were observed to decrease with increasing O-MMT content. The cationic (CTAB) and anionic (sodium dodecylsulfate) surfactants were shifted the ζ-potentials of the colloidal dispersions to more positive and more negative regions, respectively whereas nonionic surfactant (Triton X-100) caused almost no change. The pH and temperature were observed to shift the ζ-potential values of the nanocomposites to more negative and slightly more positive regions, respectively. With the addition of mono (NaCl), di ($BaCl_2$) and three ($AlCl_3$) valent salts, the ζ-potential of the nanocomposites were shifted to more negative, more positive, and much more positive regions, respectively.
 J Appl Polym Sci 123: 2911–2922, 2012

Key words: conducting polymers; nanocomposites; organoclay; polyindene; electrokinetic properties

INTRODUCTION

Polymeric materials have been synthesized by either forming systematically composites, blends or hybrid nanocomposite materials for desired engineering applications.[1] There has been considerably increasing interest on organic–inorganic nanocomposite materials in the past decade due to having characteristics of both organic and inorganic components and thus, improving the desired properties of materials for the potential applications. The conducting polymers have been the center of great interest because of their use in commercial applications such as sensors,[2] batteries,[3] molecular devices, and membranes[4] due to their electroactivity, high electrical conductivity, and stability. However, these conducting polymers usually show a poor thermal and oxidative stability and are difficult to process. The combination of these polymers and different inorganic hosts provide new opportunities to overcome the limitations mentioned above by preparing composites or so called hybrid materials which possess the properties of each of the constituent components with a synergistic effect. Nanocomposites are prepared by encapsulating a conducting polymer in an inorganic or organic matrix such as montmorillonite (MMT), graphite oxide, or carbon nanotubes to improve its engineering applicability with better dispersion stability, mechanical strength, or physical properties.[5–7]

MMT is a good candidate as inorganic host for synthesis of nanocomposite materials because of its smaller particle size, enhanced intercalation properties, unique crystal structure, which exhibits octahedral aluminate sheets sandwiched between tetrahedral silicate layers, where water or organic molecules are introduced between the layers and the layer charge can easily be controlled by exchange of cations in the galleries of MMT layers with different charges.[8] Furthermore, MMT is strongly hydrophilic, easily dispersible in water and composed of negatively charged layered plates. As a result, MMT has been used cooperatively with conductive polymers to form conductive polymer/MMT nanocomposites.

However, the combination of inorganic matrix, heterocyclic conductive polymers, and the structural changes taking place during the composite formation process are in need of exploration.[9] Among the

Correspondence to: H. I. Unal (hiunal@gazi.edu.tr).
Contract grant sponsor: Turkish Scientific and Technological Research Council; contract grant number: 107 T 711.
Contract grant sponsor: European Science Foundation (COST Action D43).

conducting polymers investigated, polyindene (PIn) has been gained much more importance during the last few years. Because of its cyclic structure, the phenyl rings present in the PIn to arrange in a horizontal fashion along the main chain, thus the repeating unit of PIn exhibits a nearly planar conformation. This unique structure provides PIn having a high T_g and special optical properties. A possible drawback of PIn is brittleness that stems from its rigidity.[10]

In colloidal systems, the electrical properties of a particle surface can be characterized by the electrokinetic measurements, so called ζ-potential. It is defined as the electrical potential at the particle double layer shear plane,[11] which may provide information on the surface complex formation at the solid/liquid interface.[12] On the other hand, the measurement of ζ-potential is also a useful parameter for understanding the colloidal stability of a system. The combination of short range-attractive van der Waals and repulsive electrostatic forces are affective on the surface of a particle. These forces form the fundamental basis for understanding of the behavior and the stability of colloidal systems, besides electrolyte content, pH value of the liquid phase and some characteristics of solid phase such as surface charge, particle size, and solid content.[13,14]

Butterworth et al. reported electrokinetic data as a function of pH for some colloidal dispersions of conducting polymer nanocomposites such as polypyrrole(PPy)-silica, polyaniline-silica, and PPy-tin(IV) oxide colloids. Their results revealed that the inorganic oxide was the major component at the particle surface which caused long-term colloidal stability.[15] Zhang and Bai reported detailed study of the ζ-potential of conductive PPy under various pH conditions. Their results revealed that the surface electric properties of PPy in aqueous solutions depend on the solution pH values; and this observation was attributed to the several factors, including the dissociation of the dopant anions (i.e., Cl^-), the selective adsorption of OH^- from the bulk solution, and the protonation/deprotonation of the nitrogen atoms on PPy structure.[12]

Therefore, it is an interesting study to investigate the possibility of preparing a colloidal PIn/O-MMT nanocomposite hybrid system. To the best of our knowledge, there has no attempt to apply MMT as an inorganic matrix to fabricate PIn/O-MMT nanocomposites. In this study, indene was *in-situ* polymerized in the presence of organically modified Na-MMT and three different compositions were obtained. The formations and morphologies of PIn/O-MMT nanocomposites were characterized by FTIR spectroscopy and SEM. XRD measurements were adopted to analyze observed the morphologies the structural changes of the host O-MMT units during the nanocomposite formation processes. Some physical properties were also determined such as: conductivity, dielectric constant, apparent density, and average hydrodynamic particle size. Furthermore, electrokinetic data were used to determine the ζ-potential characteristics of the materials. Mastery of such information will be very helpful for designing, fabricating, and developing further new nanocomposite materials based on inorganic host and heterocyclic conductive polymers.

EXPERIMENTAL

Materials

Natural bentonite was kindly supplied by Samas of Turkey; enriched in Na-content with a series of experiments by sequential precipitation and decantation processes and Na-MMT was obtained. The elemental analysis results of Na-MMT is following (wt %):

Na_2O: 3.1, MgO: 2.0, Al_2O_3: 19.9, SiO_2: 61, K_2O: 0.3, CaO: 0.8, TiO_2: 0.2, Fe_2O_3: 5.8, ignition loss: 6.9. Then Na-MMT was organically modified with CTAB, ($C_{16}H_{33}N(CH_3)_3^+Br^-$) before use. Indene (Merck) (90% pure) was distilled in vacuum (15 mmHg) prior to use. Anhydrous $FeCl_3$ (98% pure), $CHCl_3$ (99% pure), and all the other reagents were Merck products and used as received.

Synthesis of polyindene

Polyindene (PIn) was polymerized using $FeCl_3$ as an oxidizing agent and $CHCl_3$ as a solvent. The molar ratio of oxidant to monomer was taken as 1 : 1. The polymerization was carried out under $N_{2(g)}$ atmosphere at 15–20°C for 3 h. The crude PIn was filtered and then washed thoroughly several times with distilled hot water (90°C) and diethyl ether to remove any impurities present, and dried in a vacuum oven at 70°C for 48 h. The product was recovered with 90% yield.

Preparation of organo-MMT

Na-MMT was heated in a vacuum oven to 70°C for 24 h prior to use, to remove any moisture present. Dried Na-MMT (3 g) was dispersed in 250 mL deionized water at 80°C under vigorous stirring for 3 h. The suspension was ultrasonicated for 15 min and then a solution of CTAB (3.6 mmol) in 100 mL of deionized water was added dropwise into this dispersed solution, under continuous stirring. The resultant dispersion was stirred for 24 h at 80°C. Then, the dispersion was filtered and the cake obtained was thoroughly washed with deionized water. Samples of the filtrate were taken at regular intervals and tested with a solution of 0.1*M* $AgNO_{3(aq)}$ to test the presence of any residual bromide counter ions. Washing was

stopped only when the filtrate did not give a positive test to $AgNO_{3(aq)}$. The washed cake was dried in a vacuum oven at 70°C for 48 h, then grounded in a mortar and pestle and sieved through a 45-μm mesh to yield very fine, dry powder of organo-MMT.

Synthesis of PIn/O-MMT nanocomposites

PIn/O-MMT conducting nanocomposites were synthesized using $FeCl_3$ as an oxidizing agent by *in-situ* oxidative polymerization. PIn/O-MMT nanocomposites were obtained with three different PIn content and coded as: K1 [PIn(94.5%)/O-MMT(5.5%)], K2 [PIn(92.8%)/O-MMT(7.2%)] and K3 [PIn(87.9%)/O-MMT(12.1%)]. The molar ratio of oxidant to monomer was taken as 1 : 1. O-MMT was dispersed in $CHCl_3$ and ultrasonicated for 15 min for the fine dispersion of O-MMT. Then indene/$CHCl_3$ solution was added dropwise into this suspension under stirring at 55–60°C for 3 h. After the temperature was decreased to 15–20°C, $FeCl_3$ was added into this suspension under $N_{2(g)}$ atmosphere. The polymerization was carried out at 15–20°C for overnight. The precipitated PIn/O-MMT hybrid nanocomposite was washed several times with deionized hot water and diethyl ether, and then dried in a vacuum oven at 70°C for 48 h.

Characterization

Densities of the nanocomposites were measured after preparing solid pellets as discs. Conductivities and dielectric constant measurements were also carried out using those solid pellets with four-probe technique and using an HP 4192 A 6F Impedance Analyzer at $f = 1$ MHz, respectively. Particle sizes of the samples were determined by DLS using a Malvern Mastersizer E, version 1.2 b particle size analyzer. The data collected were evaluated according to Fraunhofer diffraction theory by the Malvern Software computer.[16] Magnetic susceptibility measurements were carried out using a Sherwood Scientific Model MKI Gouy scale at ambient temperature. FTIR spectra of the nanocomposites were recorded on a Mattson Model 1000 instrument as KBr discs. XRD patterns of powdered Na-MMT, O-MMT, and PIn/O-MMT nanocomposites were obtained by using a Philips PW 3717/1830 model diffractometer with Cu-Kα radiation ($\lambda = 0.51406$ nm at 40 mV and 40 mA). Thermal analysis was carried out on a Perkin Elmer Diamod TG/DTA instrument. Surface morphologies of the samples were recorded using a FEI Quanta MK2 model SEM. Element analysis of O-MMT, Pin, and PIn/O-MMT nanocomposites were determined with Elementar Analysensysteme GmbH varioMICRO CHNS model element analyzer; and Na-MMT by Rigaku model XRF instrument.

Electrokinetic studies

Zeta-potential is a physical property and represents the effective charge of dispersed particles. However, ζ-potential cannot be measured directly, but can be determined using electrokinetic techniques, such as, streaming current or potential, electrical conductivity and electrophoretic mobility.[17] ζ-potential can be converted from measured electrophoretic mobility using the Smoluchowski's equation:

$$\zeta = \frac{\eta U_E}{\varepsilon} \tag{1}$$

where ζ is the zeta-potential, ε is the dielectric permittivity of the solution (equal to $\varepsilon_0\varepsilon_r$, ε_0 being the permittivity of a vacuum, and ε_r the relative permittivity of the solution), U_E is the electrophoretic mobility of the dispersed particles, η is the viscosity of the dispersed phase.

ζ-potentials of the colloidal dispersions were measured by a Malvern Nano-ZS ζ-potential analyzer that works with Laser Doppler Electrophoresis technique. The optic unit contains a 4 mW He-Ne laser ($\lambda =$ 633 nm). The self optimization routine (laser attenuation and data collection time) in the Zeta-Sizer software was used for all the measurements. The ζ-potentials were calculated from the electrophoretic mobility using eq. (1), wherein the thickness of the electrical double layer is assumed to be smaller in comparison to the dispersed particle size. The Smoluchowski equation is an approximation valid for values of $\kappa\alpha \geq 100$, where κ is the Debye-Hückel parameter and α is the particle radius.[18,19] This approximation was accepted to be valid under the experimental conditions chosen in this research.[12,20] The electrophoretic mobility was obtained by performing an electrophoresis experiment on each of the sample and measuring the velocity of the dispersed particles using a Laser Doppler Velocimeter. For the measurements, 0.1 g sample/L colloidal dispersion was prepared in deionized water. Then the each dispersion was subjected to sonication for 30 min and held at room temperature for 2 h to establish equilibrium. Afterwards, the supernatant liquid was used for the ζ-potential measurements. The pH was adjusted immediately by a MPT-2 autotitrator unit at 25°C. In this manner, effects of time, pH, various electrolytes (NaCl, BaCl, Na_2SO_4), various surfactants [CTAB (cationic), Na-DS (sodium dodecylsulfate, anionic), Triton X-100 (nonionic)], and temperature on the ζ-potentials of the colloidal dispersions were investigated.

RESULTS AND DISCUSSION

Characterization results

A summary of the yield%, conductivity, dielectric constant, density, average particle size, and magnetic

TABLE I
Some Physical Characteristics of the Samples

Sample	Yield (%)	Conductivity (σ, S cm^{-1})	Dielectric constant	Density (d, g cm^{-3})	Average particle size ($d_{0.5}$, μm)	Magnetic susceptibility (X_g, cm g^{-1})
PIn	90	9.3×10^{-6}	4.3	1.04	1.1	3.5×10^{-6}
Na^{-}MMT	–	5.9×10^{-7}	7.5	1.88	9.2	7.5×10^{-6}
O-MMT	–	2.8×10^{-7}	6.5	1.58	5.5	6.7×10^{-6}
K1	92	5.5×10^{-6}	4.1	1.07	2.2	2.1×10^{-6}
K2	94	5.1×10^{-6}	5.8	1.08	2.3	1.7×10^{-6}
K3	95	3.7×10^{-6}	5.9	1.09	3.8	1.9×10^{-6}

susceptibility of the materials investigated in this research are given in Table I.

PIn and PIn/O-MMT nanocomposites were obtained with high yields (>90%) successfully. The conductivity of PIn was measured to be $\sigma = 9.3 \times 10^{-6}$ S cm^{-1}. The conductivities of the nanocomposites were slightly decreased with increasing O-MMT content as expected. This may be attributed to the following reasons: (i) distortion of the 3D structure of the conducting PIn chains confined between O-MMT layers, (ii) the steric hindrance of charge transfer on the PIn chains by O-MMT, and (iii) intercalation of the PIn chains between electronically nonconducting O-MMT layers which cause the formation of short conducting polymer chains. Similar behavior was reported for the dodecylbenzenesulfonic acid doped polyaniline/O-MMT,[21] poly(1-napthylamine)/MMT,[22] poly(o-methoxyaniline)/MMT[23], and poly(o-ethoxyaniline)/MMT[24] conducting nanocomposites. Besides, conductivities of the nanocomposites were also decreased with increasing O-MMT content, whereas dielectric constants, densities and average particle sizes were observed to increase. The conductivities and dielectric constants of Na-MMT and O-MMT were very close to each other. In these materials, slow acting carriers play an important role in ionic conductivity.[25] Magnetic susceptibilities of PIn and PIn/O-MMT nanocomposites were measured to be positive indicating that, the samples were paramagnetic and the conductivity mechanism was polaron in nature. These physical properties are in consistence with the properties expected from electrorheological materials, which will be published as the second part of this research.

The chemical compositions obtained from XRF analysis indicates that MMT is mainly Na-MMT, with a chemical Formula of $[(Na,Ca)_x(Al,Mg)_2(Si_4O_{10})(OH)_2.nH_2O]$ (see Table II). K and Fe elements observed in XRF analysis were mainly due to the presence of feldspar, which was also observed on the XRD traces at $2\theta = 28.5^\circ$.

TABLE II
Elemental Analysis Results of the Samples

Sample	C (%)	N (%)	H (%)	Fe (%)
PIn	91.23	–	7.07	0.8282
K1	88.05	0.16	6.76	1.2411
K2	86.42	0.13	6.61	0.25
K3	81.86	0.23	6.39	0.73

The experimental and calculated compositions obtained from the elemental analysis of O-MMT, PIn, and K1-K3 nanocomposites are given in Table II. Our calculations indicated the presence of 0.27 g CTAB/g Na-MMT. The measured compositions of PIn and PIn/O-MMT nanocomposites were observed to well agreed with the calculated values. The results indicated that residual amounts of Fe were present in the PIn and PIn/O-MMT nanocomposites arising from the presence $FeCl_4^-$ dopant counter-anions and from the structure of MMT. These results also supported the conclusion that PIn and PIn/O-MMT nanocomposite hybrid materials were successfully synthesized with the desired amounts of constituents.

FTIR spectra of PIn, O-MMT and K2 [PIn(92.8)/O-MMT(7.2)] nanocomposites showed the expected distinctive absorptions (Fig. 1).[26,27] The absorptions of PIn [Fig. 1(a)] at $\nu = 1478$–1601 cm^{-1} are due to the aromatic —C=C stretching vibrations, $\nu = 2910$–3020 cm^{-1} are typical of aromatic —C—H stretching vibrations and $\nu = 750$ cm^{-1} are due to the aliphatic C—H stretching. These absorption peaks are identical to PIn, which indicates that polymerization proceeded via —C_1 and —C_2 carbons, and the aromatic ring was protected during the polymerization and did not take part in polymerization.

FTIR spectrum of O-MMT [Fig. 1(b)] showed the bands at $\nu = 3628$, 3429, 1658, 1041, 512, and 463 cm^{-1} because of the framework O—H stretching, interlayer H_2O stretching, O—H, Si—O, Si—O—Si, and Si—O—Al bending vibrations, respectively which is common feature of natural MMT. Additionally the presence of two bands at $\nu = 2928$ and 2851 cm^{-1} are due to —CH_2 symmetric and asymmetric stretching vibrations of the CTAB.[8,28]

The FTIR spectrum of PIn/O-MMT nanocomposite [Fig. 1(c)] comprises the bands corresponding both to PIn and O-MMT; and the bands at $\nu = 3609$, 3445, 1041, 3014, 2923, 1601, 1478, and 745 cm^{-1} are

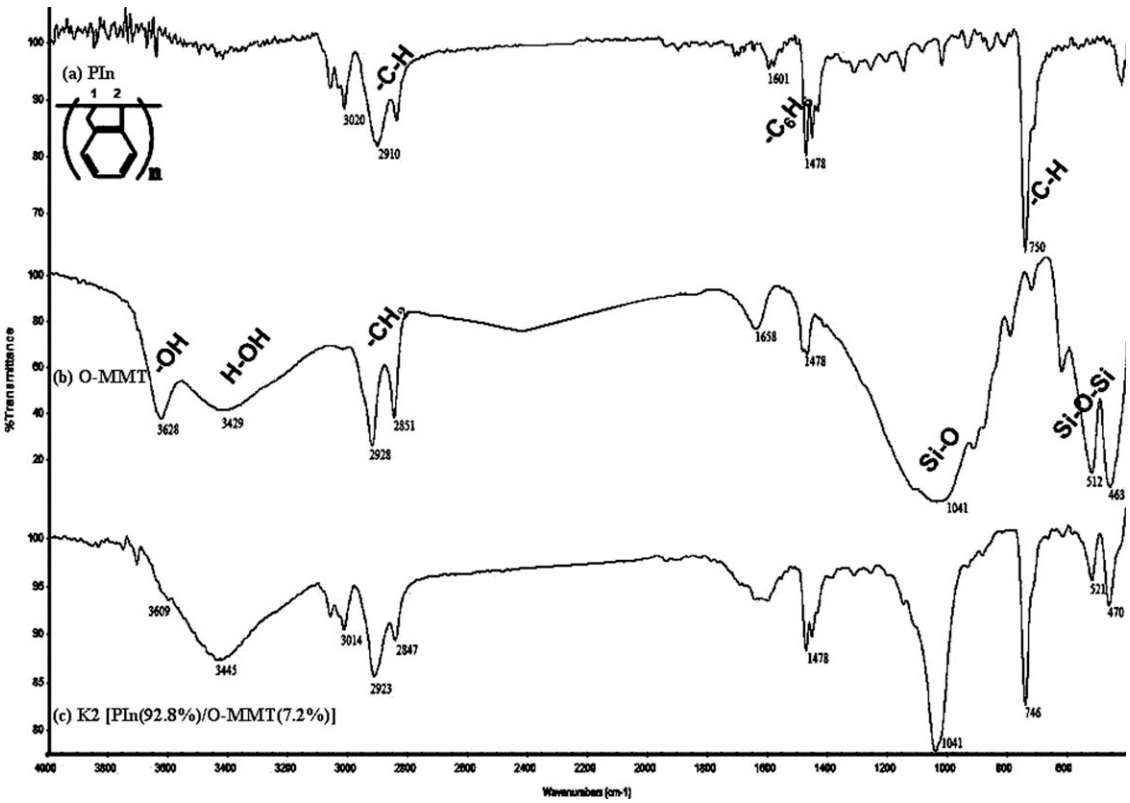

Figure 1 FTIR spectra of (a) PIn, (b) O-MMT and (c) K2: [PIn(92.8%)/O-MMT(7.2%)].

assigned to the typical of H—O—H, —OH, Si—O, aromatic —C—H, aromatic —C=C— and aliphatic —C—H stretching vibrations, respectively and gave another proof of the successful synthesis of PIn/O-MMT nanocomposite. The other K1 and K3 nanocomposites examined in this work were given the similar of FTIR spectra to K2.

XRD is widely employed for the characterization of nanocomposites formed by conducting polymers and layered silicates. As the layer spacing increases, the process can be monitored by XRD. The XRD data are used to calculate the size of crystals, degree of crystallization and spacing of layers ($d_{(001)}$) by using Bragg's equation[29]:

$$n\lambda = 2d \sin\theta \quad (2)$$

where, n is the number of layers, λ is the wave length of X-ray, d is the distance between the layers, and θ is the diffraction angle.

Figure 2 represents the XRD patterns of Na-MMT and O-MMT corresponding to $2\theta = 2$–16°. The peaks for the interlayer distance (d-space) of Na-MMT [Fig. 2(a)] and O-MMT [Fig. 2(b)] were observed at $2\theta = 7.975^\circ$ and 4.975°, respectively. To calculate the d-space, these values were introduced to the Bragg's equation. The d-space calculated for each 2θ was 1.1 nm and 1.8 nm for Na-MMT and O-MMT, respectively. The increase of d-space of O-MMT compared to the Na-MMT was due to the exchange of Na^+ and Ca^{2+} ions with CTAB cations between the interlayer of Na-MMT, which gives rise to the hydrophobicly modified Na-MMT. When the XRD pattern of O-MMT were closely examined, broadened peaks indicated that O-MMT is multilayered and d-spacing between the layers are not homogeneous, which means that CTAB molecules are inserted between the layers of Na-MMT at various directions.[30]

Figure 3 shows the XRD patterns of PIn/O-MMT nanocomposites coded as K1, K2, and K3.

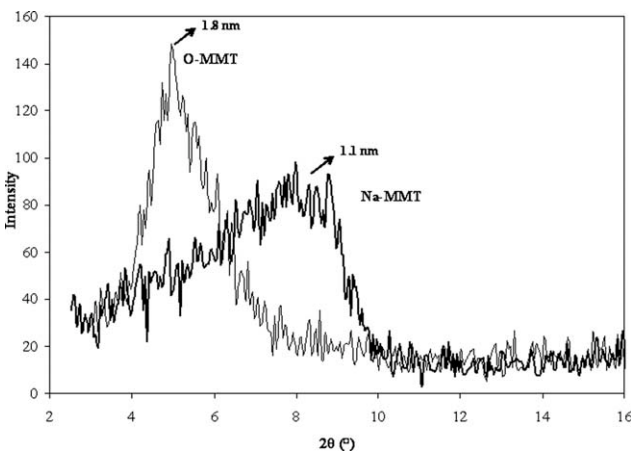

Figure 2 XRD patterns of Na-MMT and O-MMT.

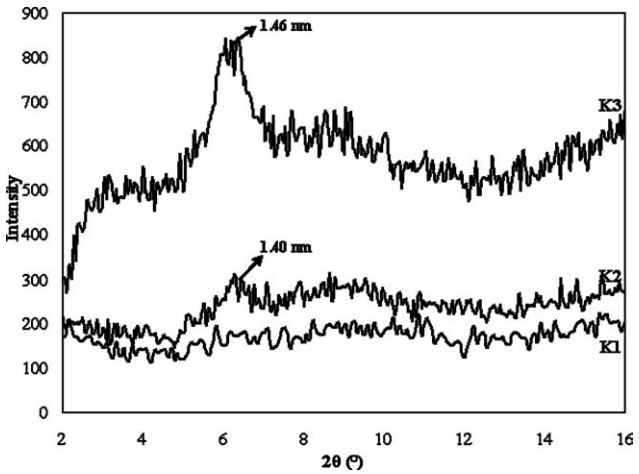

Figure 3 XRD patterns of PIn/O-MMT nanocomposites.

Disappearance of the peak on the XRD pattern of O-MMT after the formation of K1 [PIn(%94.5)/O-MMT(%5.5)] indicates a random distribution of polyindene chains between the layers of O-MMT and the total exfoliation of O-MMT structure.[31] When the amount of O-MMT increased in the K2 [PIn(%92.8)/O-MMT(%7.2)] and K3 [PIn(%87.9)/O-MMT(%12.1)] nanocomposites, two peaks were observed at $2\theta = 6.30°$ and 6.05°, respectively corresponding to the *d*-spacings of $d_{(001)K2} = 1.40$ nm and $d_{(001)K3} = 1.46$ nm. When the XRD patterns of K2 and K3 nanocomposites are compared with Na-MMT, $2\theta_{Na\text{-}MMT} = 7.975°$ shifted to $2\theta_{K2} = 6.30°$ and $2\theta_{K3} = 6.05°$, and the corresponding *d*-spacings increased from $d_{(001)Na\text{-}MMT} = 1.1$ nm to $d_{(001)K2} = 1.40$ nm and $d_{(001)K3} = 1.46$ nm. Taking these results into account, it is concluded that the PIn matrix intercalated into the widened *d*-spacing of O-MMT and resulted in with the formation of PIn/O-MMT nanocomposites successfully.[32] Same kind of XRD patterns are reported for PPy/O-MMT nanocomposites by Li et al., reporting that small amounts of PPy caused intercalation whereas, excessive amounts of PPy caused exfoliation during the nanocomposite structure.[33]

A summary of thermal analysis results of Na-MMT, O-MMT, PIn, K1, K2, and K3 nanocomposites are given in Table III, besides TGA thermograms of the K1, K2, and K3 nanocomposites are given in Figure 4. PIn chains decomposes with one step weight loss between 342 and 395°C with a half life temperature of 379°C and residue of 28 wt % at 900°C. T_g of PIn was also recorded from a DSC thermogram and determined to be 200°C (on set). Mano and Calafate reported $160 \leq T_g \leq 220$ values during the electroinitiated polymerization of indene and acenaphthylene[34] and also Kennedy et al.[26] and Tsunogae et al.[35] reported 200°C T_g for PIn during the living polymerization and living carbocationic copolymerization of indene, respectively, which supports the T_g value observed for PIn in our study.

TABLE III
Thermal Analysis Results of the Samples

Sample	Decomposition temperature (°C)				Residue at 900°C (% m/m)
	[a]T_i	[a]T_m	[a]T_f	[a]$T_{d\ (1/2)}$	
MMT	551	619	642	–	88
O-MMT	246	296	351	–	73
	423	394	602		
PIn	342	374	395	379	28
K1	333	372	397	377	30
K2	328	362	393	377	32
K3	326	355	385	376	35

[a] T_i, initial; T_m, maximum; T_f, final; $T_{d(1/2)}$: half-life of decomposition temperatures.

Na-MMT decomposes with three step weight losses. The first step weight loss (4 wt %) occurs below 110°C due to the adsorbed water on the surface. The second step occurs between 110 and 250°C corresponding to 6 wt % loss due to the removal of H_2O molecules from the interlayer coordinated to the cations (dehydration). The third step occurs between 551 and 642°C corresponding to 3 wt % loss due to the decomposition of H-bonded water molecules and some of the —OH groups from the tetrahedral sheets of Na-MMT (dehydroxylation).[36] The residual Na-MMT was 88 wt % at 900°C.

O-MMT has four-step weight losses. The first weight loss occurs below 110°C corresponding to <3 wt % loss due to adsorbed H_2O molecules on the surface. The second weight loss occurs at 110–220°C corresponding to 2 wt % due to the bonded H_2O molecules between the layers (dehydration). The organophilic properties of the O-MMT lead to the conclusion that the alkylammonium ions adsorbed less H_2O molecules when compared with Na-MMT indicating that modification of Na-MMT was successful.[37] The third step occurs at 246–351°C corresponding to 8 wt % loss

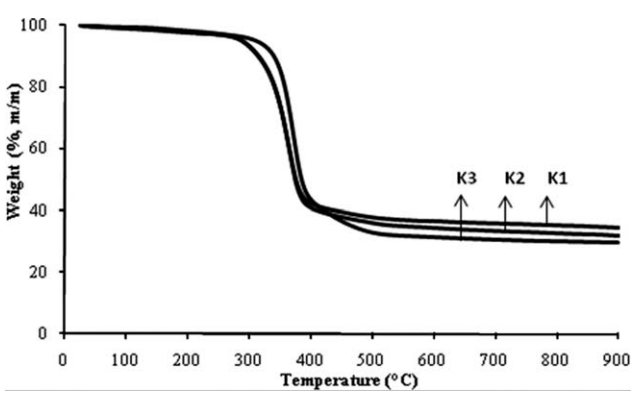

Figure 4 TGA thermograms of the K1, K2, and K3 nanocomposites.

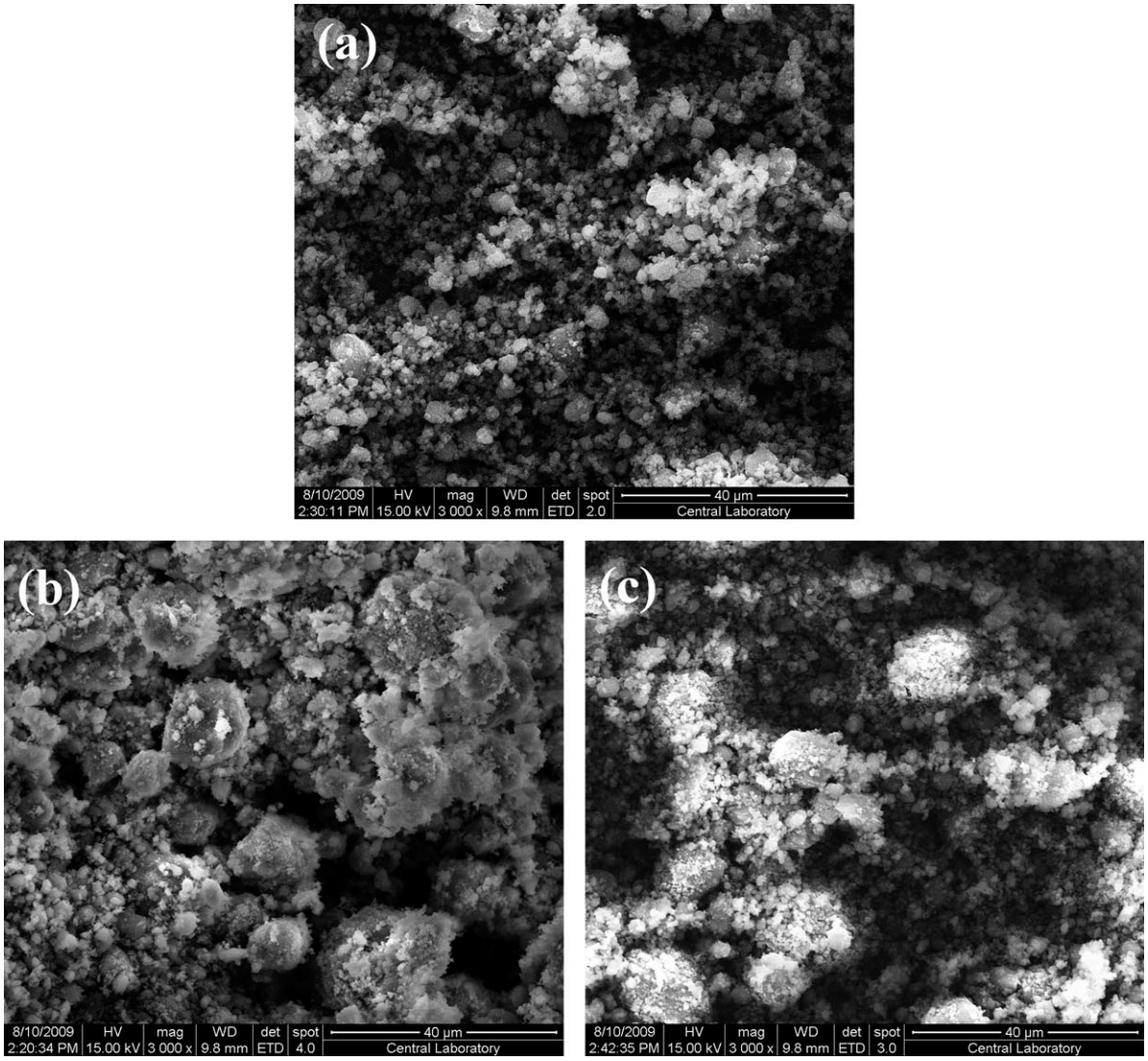

Figure 5 SEM micrographs of (a) PIn, (b) O-MMT, and (c) K2.

due to decomposition of CTAB. The final step occurs at 423−602°C corresponding to 4 wt % loss due to the crystalline H_2O molecules in O-MMT structure as well as continuing decomposition of CTAB. The residue of O-MMT was 73 wt % at 900°C.

PIn/O-MMT nanocomposites decomposed at one-step weight loss (Table III and Fig. 4). The initial decomposition temperatures of the nanocomposites were decreased when compared with PIn, due to the flammable remaining surfactants on the structure of nanocomposites, which is also supported with increasing amount of O-MMT in the composition of the nanocomposites. PIn is a thermally stable polymer. When initial residue values at 900°C were taken into account, PIn/O-MMT nanocomposites have gained more thermal stability than PIn with increasing amount of O-MMT, which was one of the aims of this study. Wang et al. reported similar behavior on TGA analysis of ABS/MMT nanocomposite.[38] On the other hand, initial decomposition temperatures of K1-K3 nanocomposits were higher than O-MMT and closer to PIn, which is another indication of enhanced thermal stability of the nanocomposites.

Figure 5(a–c) shows SEM micrographs of PIn, O-MMT, and K2 respectively. The SEM micrograph of PIn [Fig. 5(a)] shows a closely packed, porous structure with varying particle sizes, which is consistent with literature.[39] SEM micrograph of O-MMT [Fig. 5(b)] shows multilayered and spherical in shape structure with varying sizes having sponge-like CTAB surfactants on their surfaces. SEM micrograph of PIn/O-MMT nanocomposite shows granular and porous structure demonstrating that O-MMT particles are homogeneously surrounded with PIn particles [Fig. 5(c)]. Further, in combination with XRD patterns, PIn chains are not only produced inside the O-MMT interlayer spaces but also on the surfaces of O-MMT. The other composites (K1 and K3) were also shown the identical SEM micrographs to K2.

Zeta-potential results

Zeta potential, the potential between the slipping plane and the bulk solution, is an important electrokinetic property of dispersed particles which has traditionally been applied to estimate the stability of colloidal dispersions.[40] A common way to evaluate the stability of colloidal dispesions and to understand the type of surface charge is by determining the electrophoretic mobility, which can then be used to calculate the magnitude of ζ-potential. In dispersions where value of the ζ-potential is closer to zero (isoelectronic point, IEP) particles tend to agglomerate. Depending on the type of the dispersed phase, at highly negative or positive values of ζ-potential, particles in dispersions tend to repel each other, which results with agglomeration free colloidally stable dispersions. The actual values needed to prevent reagglomeration are in dispute, and depend on the composition of the surrounding solvent, concentration of the ions, types of the surfactants, pH value of the environmental, time, temperature, and presence of the functional groups or chemical composition on the surface of the dispersed particles. The effects of these parameters onto the magnitude of ζ-potentials of the studied materials in this research are discussed below.

Effect of time on pH

To determine the pH profile of the samples, the effect of time on pH of the colloidal dispersions prepared from Na-MMT, Pin, and K2 [PIn(92.8)/O-MMT(7.2)] in aqueous media are given in Figure 6. The initial pH of Na-MMT was measured to be 7.83 and reached to the equlibrium value of 7.02 at the end of 120 min, which may be attributed to the formations of $-SiO^-$ or $-AlO^-$ from deprotonation of $-SiOH$ or $-AlOH$ sites resulting in negative charges at the edges in the lattice of the Na-MMT particles.

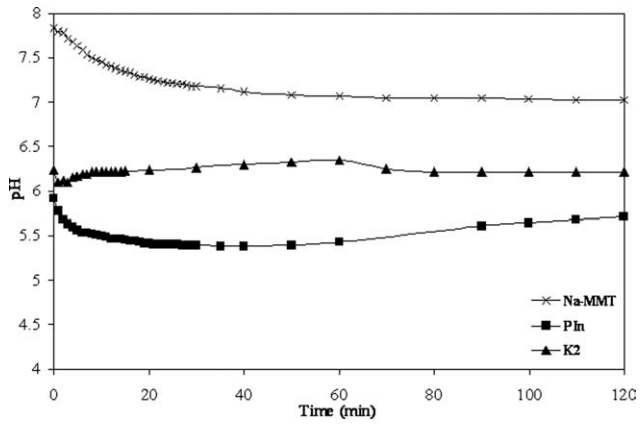

Figure 6 The effect of time on pH profile of Na-MMT, Pin, and K2 colloidal dispersions.

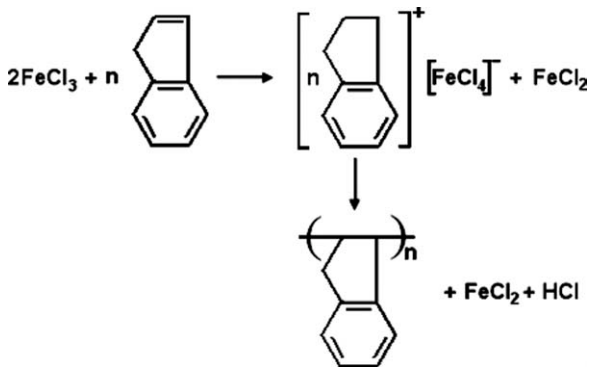

Scheme 1 Chemical polymerization of indene.

The initial pH of PIn was measured to be 5.92 and reached to the equilibrium value of 5.71 at the end of 120 min. This slight decrease in pH may be attributed to the reduced amount of OH^- ions in the solution due to the exchange taking place with dopant anions (coming from $FeCl_4^-$, see Scheme 1).

Conversely, when we look at the pH profile of the K2 [PIn(92.8)/O-MMT(7.2)], initial pH was measured to be 6.24 and reached to the equilibrium value of 6.21 at the end of 120 min showing a very stable behavior. It was concluded that the samples reached to the ionic equilibria at the end of 120 min. Thus, for the rest of the study, the colloidal dispersions were prepared and hold for 120 min, then subjected to ζ-potential measurements.

Effect of pH on ζ-potentials

To determine the effect of pH on ζ-potentials of the samples, a series of experiments were conducted on dispersions prepared from Na-MMT, Pin, and K1-K3 nanocomposites and results obtain are depicted in Figure 7 and also summarized in Table IV.

The ζ-potential values of Na-MMT were observed to change in a narrow range ($\zeta_{pH\,=\,3.21} = -16$ mV, and $\zeta_{pH\,=\,9.8} = -43$ mV) when compared with the other samples studied, which may be attributed to the H_3O^+ adsorption on the negatively charged

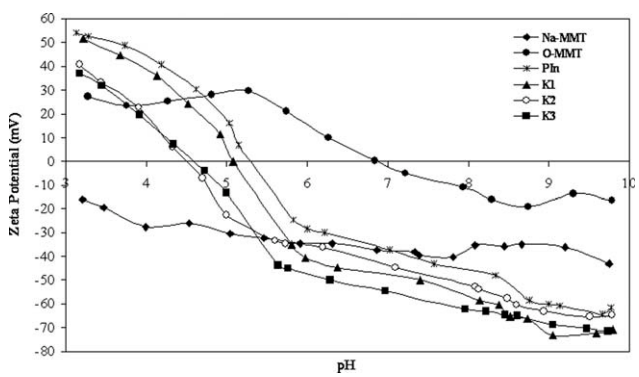

Figure 7 The effect of pH on ζ-potentials of the samples.

TABLE IV
ζ-Potential Values of the Samples at Different pHs

Sample	$pH_{initial}$	$\zeta_{initial}$ (mV)	pH_{min}	ζ at pH_{min} (mV)	pH_{max}	ζ at pH_{max} (mV)	pH_{IEP}
Na-MMT	7.8	−40.4	3.2	−16.0	9.8	−37.8	–
O-MMT	7.6	12.5	2.4	28.1	9.8	−16.4	4.4
PIn	7.1	−40.8	3.1	54.2	9.8	−61.4	5.3
K1	7.3	−42.2	3.2	51.6	9.8	−70.7	5.1
K2	7.4	−38.4	3.2	40.8	9.8	−64.4	4.5
K3	6.7	−23.8	3.2	37.0	9.7	−71.4	4.6

surface of Na-MMT at lower pH values. On the other hand, an IEP was not determined for the Na-MMT in the pH range examined. These results are in agreement with the published results on Na-MMT by the other researchers.[41–43]

The ζ-potential values of O-MMT were observed to shift to more positive regions when compared with Na-MMT. This may be attributed to the strong electrostatic interactions between cationic CTAB and negatively charged Na-MMT particles; CTAB ions are adsorbed on the Na-MMT particles via cation exchange and adsorption mechanisms. Marras et al. reported that at low surfactant loading levels, surfactant ions were adsorbed inside the interlayer spaces through the cation exchange (not occurring in the positive surface charge). However, as the loading of surfactant ions increased, they were adsorbed into the layers via cation exchange and onto the surfaces by means of hydrophobic bonding. Hydrophobic bonding is defined as the mutual hydrophobic attraction between the alkyl chains (tails) of surfactant molecules and the tendency of the hydrophobic tails to be removed from water, resulting positive charges on the surfaces of Na-MMT clay particles.[44,45]

We observed a wide ζ-potential change and IEP for $PIn_{(aq)}$ dispersions. The counter dopant anions ($FeCl_4^-$) present on the PIn structure (Scheme 1) surrounds the PIn chains and results in with a negative ζ-potential value ($\zeta = -24$ mV, $pH_{initial} = 5.71$). As the pH was decreased, by adding H_3O^+ ions into the dispersion medium, $FeCl_4^-$ anions were surrounded with positive charges and ζ-potential values shifted to more positive regions, by passing through the IEP at pH = 5.31 and reaching to $\zeta = 54$ mV at pH = 3.13. When a base ($NaOH_{(aq)}$) was introduced into the dispersion medium, OH^- anions increased the number of negative charges present in the medium, shifted the ζ-potential value to more negative regions and reached to $\zeta = -62$ mV at pH = 9.77.

When the change of ζ-potentials of K1−K3 nanocomposite dispersions with pH was considered, it was observed that ζ-potential values shifted to relatively more negative regions than PIn with the presence of O-MMT and increasing pH of the medium.

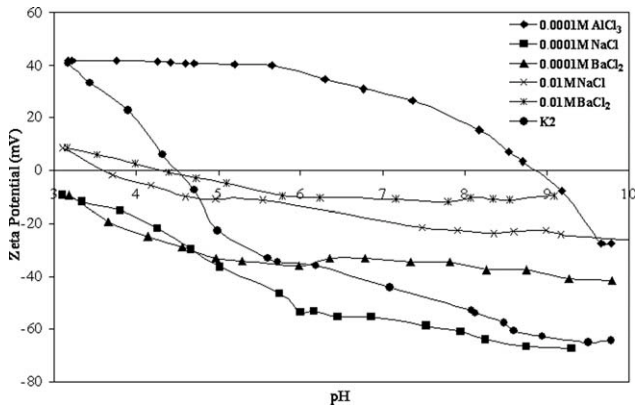

Figure 8 The effect of cationic salts on ζ-potentials of K2 nanocomposite/aqueous colloidal dispersions.

The ζ-potential values of all the PIn/O-MMT composites examined in this work were observed to increase with increasing PIn content, increasing conductivity, and decreasing dielectric constant of the dispersed particles (see Table IV). As the H_3O^+ ions were introduced into the dispersion medium, IEP of the nanocomposites were observed to shift to the lower pH regions by increasing O-MMT content and persisting in the acidic region. The ζ-potential values of the nanocomposites were observed to change in the following order at the lowest pH values: ($\zeta_{K3(pH\,=\,3.17)} = 37$ mV $< \zeta_{K2(pH\,=\,3.17)} = 41$ mV $< \zeta_{K1(pH=3.22)} = 52$ mV). It was concluded that PIn/O-MMT nanocomposites perfectly meet the minimum requirements of colloidal stability ($+30$ mV $\leq \zeta \leq -30$ mV)[46] especially at basic media, which is an important experimental result from industrial applications points of view.

Effect of electrolytes on ζ-potentials

The effect of cationic (Na^+, Ba^{2+}, Al^{3+}) and anionic (Cl^-, SO_4^{2-}) salts on the ζ-potentials of K2 nanocomposite/aqueous colloidal dispersions are depicted in Figures 8 and 9, respectively. As reflected from

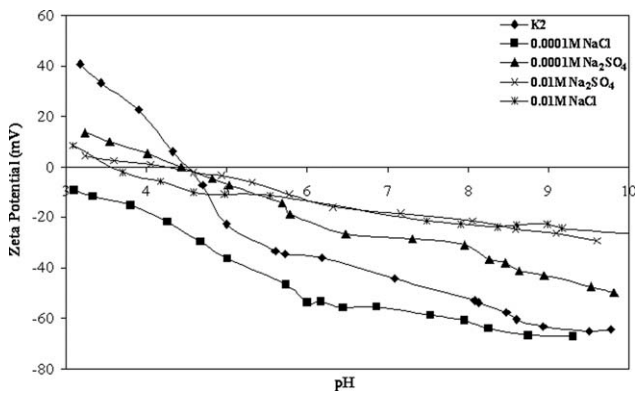

Figure 9 The effect of anionic salts on ζ-potentials of K2 nanocomposite/aqueous colloidal dispersions.

Figure 8, ζ-potential values of K2 were observed to shift to more negative regions when $c = 1 \times 10^{-4}$ *M* $Na^{+}_{(aq)}$ monovalent cation added into the medium. When the concentration of $Na^{+}_{(aq)}$ increased 100 times ($c_{NaOH} = 1 \times 10^{-2}$ M), the ζ-potential values were observed to shift to more positive regions due to the increase in ionic strength of the colloidal dispersion and compression of the diffuse layer by $Na^{+}_{(aq)}$ cations. It was observed that, divalent (Ba^{2+}) and three valent (Al^{3+}) cations increased the ionic strength of the colloidal dispersions more than monovalent (Na^{+}) cation, compressed the electrical double layer and shifted the ζ-potential values to more positive regions. The IEPs were recorded to be at the pH values of 4.7, 3.7, 4.4, and 9.2 for virgin $K2_{(aq)}$, after the additions of 1×10^{-2} *M* Na^{+}, Ba^{2+} and 1×10^{-4} *M* Al^{3+} salts into this colloidal dispersion, respectively. It was concluded that mono and divalent cations did not change the surface charges of the K2 dispersions, whereas, three valent Al^{3+} cations caused changes on the surface charges of K2 dispersions and shifted the ζ-potential values to more positive regions. These observations agree well with the Gouy-Chapman model which states that monovalent cations cause more negative ζ-potential values than in pure water, since they exchange with H_3O^{+} present in the medium which expands the electrical double layer. Our observations are also in accordance with the results reported by Yukselen et al. on a ζ-potential study of kaolinite that divalent cations cause smaller ζ-potential values than the monovalent ones.[47]

Since $Q_{sp} > K_{sp}$ is valid for 1×10^{-2} *M* $Al^{3+}_{(aq)}$ concentration, it was impossible to observe a pH change due to the starting precipitation of $Al(OH)_3$ in the colloidal dispersion medium. On the other hand, when we look at the effect of monovalent and divalent anions on the ζ-potential values of $K2_{(aq)}$ dispersions, $c = 10^{-4}$ *M* $Cl^{-}_{(aq)}$ ions shifted the ζ-potentials to relatively more negative values, whereas $c = 10^{-4}$ *M* and 10^{-2} *M* $SO^{2-}_{4\,(aq)}$ ions shifted the ζ-potentials to relatively more positive regions (Fig. 9). Besides, when the concentration of anions increased in the dispersion medium, ζ-potentials that are more positive were recorded. The action of the ions in the diffuse layer, which have the same charge with the dispersed particles in the dispersion, compress the electrical double layer and thus reduce the value of ζ-potential and as a result reduce the interparticle repulsion that keep the particles suspended inside the colloidal dispersion. Thickness of the electrical double layer (κ^{-1}) was related to the ionic strength of a colloidal dispersion in water at 25°C as following[48]:

$$\frac{1}{\kappa} = \frac{3}{Zc^{1/2}} \quad (3)$$

where *Z* and *c* are the valency of the ion and the ion concentration of the colloidal dispersion, respectively. This formula indicates that for the same anion concentration, the valency of anion contribute significantly to the thickness of double layer and consequently causes a reduction in the ζ-potential of the PIn/O-MMT aqueous colloidal dispersions.

Effect of surfactants on ζ-potentials

When a cationic surfactant (CTAB) was added into the $K2_{(aq)}$ colloidal dispersions, the surfaces of K2 particles covered with positively charged cations and ζ-potential values ended up with 42 mV at $c_{CTAB} = 20$ ppm by passing through an IEP at $c_{CTAB} = 0.67$ ppm (Fig. 10).

When an anionic surfactant (Na-DS) was added into the $K2_{(aq)}$ colloidal dispersions, which has an already negatively charged surface due to $FeCl^{-}_{4}$ dopant counter-anions, ζ-potential values ended up at −61 mV at $c_{Na\text{-}DS} = 20$ ppm, without passing through an IEP.

Conversely, addition of a nonionic surfactant (Triton X-100) into $K2_{(aq)}$ dispersions caused no observable change on the ζ-potential, within the experimental limits, which indicates that, no significant change occurs on the thickness of the electrical double layer around the dispersed $K2_{(aq)}$ colloidal particles.

Effect of temperature on ζ-potentials

Temperature increments observed to cause little increase on the ζ-potential of $K2_{(aq)}$ colloidal dispersions, which is started with −41 mV at 5°C and ended up with −36 mV at 50°C corresponding to a 5 mV shift towards the positive region (Fig. 11). Since the temperature has an effect on various parameters

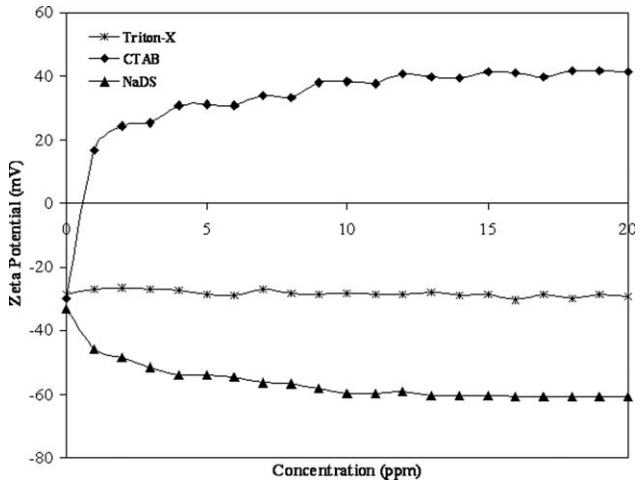

Figure 10 The effect of surfactants on ζ-potentials of K2 nanocomposite/aqueous colloidal dispersions.

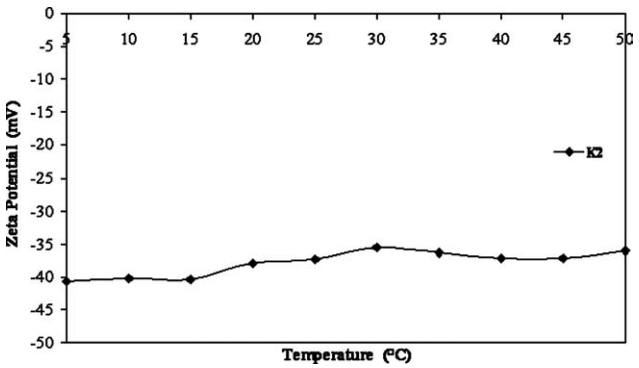

Figure 11 The effect of temperature on ζ-potentials of K2 nanocomposite/aqueous colloidal dispersions.

i.e., viscosity, dielectric constant, and ion adsorption; it also has an effect on ζ-potential values. An increase in temperature reduces the electrical double layer thickness, due to the decrease in viscosity of the medium and should thereby reduce the colloidal stability of the dispersed PIn/O-MMT particles. Temperature can also affect the surface potential of the colloidal particles by readily displacing the equilibrium between the ionized groups and the medium.[49]

CONCLUSIONS

Polyindene/O-MMT conducting nanocomposite hybrid materials, having three different compositions, were successfully synthesized by *in-situ* oxidative polymerization using $FeCl_3$. Their spectral, thermal, optical characterizations, and some physical properties were investigated. TGA analysis revealed that, PIn/O-MMT nanocomposites had more thermal stability than PIn homopolymer as desired. From the XRD results both exfoliation and intercalation were determined for PIn/O-MMT nanocomposites. SEM results revealed that PIn chains were homogeneously distributed between the O-MMT layers. Paramagnetic behaviors were detected for the PIn/O-MMT nanocomposites and their conductance mechanism was decided to be polaron in nature with the conductivity ranging between 3.7×10^{-6}–5.5×10^{-6} S cm^{-1}, which were gradually reduced with the inclusion of the O-MMT into the nanocomposite structure and brought well into the range of electrorheological active materials. ζ-potential measurements demonstrated that PIn, K1, K2, and K3 nanocomposites have enough colloidal stability and perfectly suitable for potential industrial applications, especially in basic media, in the presence of multivalent cations, ionic surfactants, and high temperature conditions. Finally, the conducting nanocomposites were observed to sensitive to external electric field strength and classified as smart materials having a potential for industrial vibration damping applications, which will be published soon as a second part of this study.

References

1. Fang, F. F.; Choi, H. J.; Joo, J. J Nanosci Nanotechno 2008, 8, 1559.
2. Kulkarni, M. V.; Athawale, A. A. J Appl Polym Sci 2001, 81, 1382.
3. Nakajima, T.; Kawagoe, K. Synthetic Met 1989, 28, 629.
4. Galloppa, A.; Catalog, F.; Campoli, F.; Beccherelli, R.; Dalessandro, A.; Ferrara, V.; Maltese, P. Mol Cryst Liq Cryst 1996, 290, 129.
5. Gopalan, A. I.; Lee, K. P.; Santhosh, P.; Kim, K. S.; Nho, Y. C. Compos Sci Technol 2007, 67, 900.
6. Wang, J.; Xu, Y.; Chen, X.; Sun, X. Compos Sci Technol 2007, 67, 2981.
7. Boukerma, K.; Piquemal, J. Y.; Chehimi, M. M.; Mravcakova, M.; Omastova, M.; Beaunier, P. Polymer 2006, 47, 569.
8. Erol, O.; Unal, H. I.; Sari, B. Polym Compos 2010, 31, 471.
9. Han, Y.; Lu, Y. Compos Sci Technol 2009, 69, 1231.
10. Kanaoka, S.; Ikeda, N.; Tanaka, A.; Yamaoka, H.; Higashimura, T. J Polym Sci Pol Chem 2002, 40, 2449.
11. De Medeiros, D. W. O.; Dos Santos, D. S.; Dantas, T. N. C.; Pereira, M. R.; Giacometti, J. A.; Fonseca, J. L. C. Mater Sci-Poland 2003, 21, 251.
12. Zhang, X.; Bai, R. Langmuir 2003, 19, 10703.
13. Pashley, R. M.; Karaman, M. E. Applied Colloid and Surface Chemistry; Wiley: Chichester, 2004.
14. Schwarz, S.; Buchhammer, H. M.; Lunkwitz, K.; Jacobasch, H. J Colloids Surf A 1998, 140, 377.
15. Butterworth, M. D.; Corradi, R.; Johal, J.; Lascelles, S. F.; Maeda, S.; Armes, S. P. J Colloid Interface Sci 1995, 174, 510.
16. German, R. M. Powder Metallurgy Science; Material Powder Industries Federation: Princeton, 1994.
17. El-Gholabzouri, O.; Cabrerizo-Vilchez, M. A.; Hidalgo-Alvarez, R. Colloid Surface A 2006, 291, 30.
18. Elaissari, A. Colloidal Polymers; Marcel Dekker: New York, 2003.
19. Kosmulski, M. Chemical Properties of Material Surfaces; Marcel Dekker: New York, 2001.
20. Kelly, T. L.; Che, S. P. Y.; Yamada, Y.; Yano, K.; Wolf, M. O. Langmuir 2008, 24, 9809.
21. Jial, W.; Segal, E.; Kornemandel, D.; Lamhot, Y.; Narkis, M.; Siegmann, A. Synthetic Met 2002, 128, 115.
22. Ashraf, S. M.; Ahmad, S.; Riaz, U. J Macromol Sci B 2006, 45, 1109.
23. Yeh, J. M.; Chin, C. P. J Appl Polym Sci 2003, 88, 1072.
24. Yeh, J. M.; Chen, C. L.; Chen, Y. C.; Ma, C. Y.; Lee, K. R.; Wei, Y.; Li, S. Polymer 2002, 43, 2729.
25. Esmer, K. Mater Lett 1998, 34, 398.
26. Kennedy, J. P.; Midha, S.; Keszler, B. Macromolecules 1993, 26, 424.
27. Hahn, S. F.; Hillmyer, M. A. Macromolecules 2003, 36, 71.
28. Tunc, S.; Duman, O. Colloid Surface A 2008, 317, 93.
29. Ke, Y. C.; Stroeve, P. Polymer-Layered Silicate and Silica Nanocomposites; Elsevier: Amsterdam, 2005.
30. Gitipour, S.; Bowers, M. T.; Bodocsi, A. J Colloid Interface Sci 1997, 196, 191.
31. Bae, W. J.; Kim, K. H.; Jo, W. H.; Park, Y. H. Polymer 2005, 46, 10085.
32. Ballav, N.; Sardar, P. S.; Ghosh, S.; Biswas, M. J Mater Sci 2006, 41, 2959.
33. Li, T.; Zeng, X.; Xu, J. Polym-Plast Technol 2007, 46, 751.
34. Mano, E. B.; Calafate, B. A. L. J Polymer Sci Polymer Chem Ed 1981, 19, 3325.
35. Tsunogae, Y.; Majorous, I.; Kennedy, J. P. J Macromol Sci A 1993, 30, 253.

36. Bray, H. J.; Redfern, S. A. T.; Clark, S. M. Mineral Mag 1998, 62, 647.
37. Chen, K. H.; Yang, S. M. J Appl Polym Sci 2002, 86, 414.
38. Wang, S.; Hu, Y.; Song, L.; Wang, Z.; Chen, Z.; Fan, W. Polym Degrad Stabil 2002, 77, 423.
39. Sarikaya, S.; Yavuz, M.; Yilmaz, H.; Unal, H. I.; Sari, B. Polym Compos 2009, 30, 583.
40. Zadaka, D.; Radian, A.; Mishael, Y. G. J Colloid Interface Sci 2010, 352, 171.
41. Duran, J. D. G.; Ramos-Tejada, M. M.; Arroyo, F. J.; Gonzalez-Caballero, F. J Colloid Interface Sci 2000, 229, 107.
42. Sondi, I.; Milat, O.; Pravdic, V. J Colloid Interface Sci 1997, 189, 66.
43. Duman, O.; Tunc, S. Micropor Mesopor Mat 2009, 117, 331.
44. Marras, S. I.; Tsimpliaraki, A.; Zuburtikudis, I.; Panayiotou, C. J Colloid Interface Sci 2007, 315, 520.
45. Xu, S.; Boyd, S.A. Environ Sci Technol 1995, 29, 312.
46. Malvern Instruments Ltd. Zetasizer Nano series technical note, MRK654–01.
47. Yukselen, Y.; Kaya, A. Water Air Soil Poll 2003, 145, 155.
48. Usui, S. In Electrical Phenomena at Interfaces Fundamentals, Measurements, and Applications; Kitahara, A.; Watanabe, A., Eds.; Marcel Dekker: New York, 1984.
49. Garcia-Garcia, S.; Jonsson, M.; Wold, S. J Colloid Interface Sci 2004, 298, 694.